THE ASTROPHYSICAL JOURNAL, 353:24–33, 1990 April 10

QUASAR COLORS: STATISTICS AND COSMOLOGICAL EVOLUTION

EMANUELE GIALLONGO
Osservatorio Astronomico di Roma, Italy
AND
DARIO TREVESE
Istituto Astronomico, Università di Roma "La Sapienza," Italy
Received 1989 April 10; accepted 1989 October 9

ABSTRACT

We have constructed a model spectrum to study QSO broad-band colors as a function of redshift. Using the available statistical data, we have generated realistic color distributions that give quantitative estimates of the incompleteness associated with the various color selection techniques as a function of redshift. We have also developed a simple model for the average Lyman continuum absorption based on the statistics of the Lyα clouds to explore the resulting colors of high-redshift QSOs. Selection biases on the estimate of QSO density at high redshift are also discussed.

Subject headings: cosmology — quasars — spectrophotometry

I. INTRODUCTION

A powerful tool to investigate the nature of the quasar phenomenon is the statistical study of the cosmological evolution of the luminosity function, i.e., the population distribution over the luminosity-redshift plane.

This requires the use of statistical samples as well as a reliable estimate of the selection effects associated with the various observational techniques.

The available samples of candidates are based mainly on color photometry or multiobject spectroscopy. Variability and absence of proper motions are also used as complementary information. In any case, medium-resolution spectroscopy is required to confirm the candidates and to establish redshifts.

The first statistical sample of optically selected QSOs was based on the ultraviolet excess (UVX) criterion (Braccesi, Formiggini, and Gandolfi 1970). The redshift distribution of UVX samples drops at $z \gtrsim 2$, and spectroscopic surveys were necessary to demonstrate that the lack of higher redshift objects is a selection effect and not a real cutoff (Osmer and Smith 1980).

A new selection method based on broad-band colors was introduced by Koo and Kron (1982). They used $U-J$ and $J-F$ to define as QSO candidates the objects lying outside the stellar locus in this color-color plane. Spectroscopy of QSO candidates proved that this method successfully overcomes the limits of UVX selection, allowing an extension to early cosmic times of the analysis of the luminosity function.

Marano, Zamorani, and Zitelli (1988, hereafter MZZ) applied the same method, obtaining counts in good agreement with Koo, Kron, and Cudworth (1986, hereafter KKC) results. Adding grism images, they also found some high-redshift ($z > 2$) objects lost by the color selection.

QSOs with $z \gtrsim 3.5$ have been found on objective prism plates (Hazard and McMahon 1985) and in grism transit surveys (Schmidt, Schneider, and Gunn 1987). The findings are consistent with a gradual decline of the comoving quasar density beyond $z \sim 3$. However, the relevant selection effects are difficult to evaluate. The highest z QSOs known at present ($z \sim 4.4$) have been found by Warren *et al.* (1987*a*), using wide field plates and multicolor (*UBVRI*) techniques which extend the Koo and Kron (1982) criterion. The QSO surface density is roughly consistent with the spectroscopic results; however, drawing out of the data the evolution of the luminosity function entails an accurate estimate of the incompleteness involved at each redshift.

QSO paths in color space as a function of redshift have been computed in the past using model spectra (Schmidt 1968; Braccesi, Formiggini, and Gandolfi 1970; Véron 1983). Recently, Koo and Kron (1988) have also included a schematic non-evolving representation of the Lyα absorption to evaluate the K-correction in the blue band.

Possible colors at high redshifts have also been investigated by Miller and Mitchell (1988) using schematic spectra.

The statistical distribution of the spectral properties is not taken into account in any of the above models. In the present work, we construct a model spectrum, accurate enough for the specific purpose of computing broad-band colors, containing the statistical information now available about the main emission lines (Baldwin, Wampler, and Gaskell 1989) and the main continuum features. The aim is to compute the statistical distribution of colors and evaluate the completeness of color-selected samples.

At $z \gtrsim 2.8$, the Lyman continuum absorption enters the U band, and the position of QSOs becomes uncertain, because the properties of the intergalactic medium are poorly known. However, on the basis of the recent results of Steidel and Sargent (1987) and Sargent, Steidel, and Boksenberg (1989) about the statistics of the absorbing clouds, we can compute an average absorption evolving with redshift and depending on the cloud properties.

In § II, we illustrate our model spectrum and the relevant parameters. In § III, we discuss the K-corrections and QSO paths in color-color diagrams with special attention to high-z QSOs. Finally, in § IV we estimate statistical confidence regions in color-color diagrams and their implications for completeness levels of QSO color surveys.

II. MODEL SPECTRUM

a) Continuum Shape

The QSO continuum spectral energy distribution between the near-infrared ($\lesssim 10{,}000$ Å) and the soft X-ray ($E \sim 2$ keV) can be represented by three components (e.g., Elvis 1986):

1. an IR-X power-law $f_\nu \sim \nu^{-\alpha}$ with $\alpha \sim 1$;
2. a big blue bump extending from ~ 5000 Å to extreme UV and in some cases towards soft-X band, probably of thermal origin (Malkan and Sargent 1982; Malkan 1983) well represented (for our limited use) between 5000–1000 Å by a blackbody emission at a single temperature $T_{BB} \sim 30{,}000$ K;
3. a small 3000 Å bump due to thin Balmer continuum emission at $T_{BC} \sim 12{,}500$ K (Grandi 1982).

Detailed fitting, however, is available only for a small number of objects. In the absence of more information, we conservatively assume a uniform statistical distribution of model parameters in a range equal to twice the rms dispersion.

From Malkan and Sargent (1982) and Malkan (1983), we have $\alpha = 1 \pm 0.1$ for the power-law index, $F_{BB}/F_{pl} = 0.37 \pm 0.22$ (flux ratio at 5500 Å of the blackbody to power-law emission), and $T_{BB} = 27{,}800 \pm 5540$ K for the temperature. From Grandi (1982), we have taken $T_{BC} = 12{,}500$ K and $F_{BC}/F_{H\alpha} = 1.25$ (the flux ratio of Balmer continuum to Hα emission line). Dispersion of Balmer continuum is assumed as a result of Hα dispersion.

Finally, we neglect the reddening internal to the QSO because of the weak 2200 Å absorption dip usually observed (see, e.g., Richstone and Schmidt 1980; Malkan and Sargent 1982).

b) *Emission-Line Spectrum*

An emission-line spectrum is superposed on the continuum. This contains the main lines taken from a recent statistical investigation by Baldwin, Wampler, and Gaskell (1989). They present spectrophotometry of two complete samples of quasars: radio selected and color selected, respectively. We have reevaluated statistical correlations between logarithms of continuum luminosity and rest equivalent widths in the standard ($q_0 = 0.1$) Friedmann cosmology. Linear regression parameters together with rms dispersions of the points around the mean linear regression are shown in Table 1. Moreover, we have added the Balmer lines ratios and some minor emission lines taken from Grandi (1982) (see his Table 1). Statistical variances of these lines are simply due to the variance of Hβ line obtained from the Baldwin, Wampler, and Gaskell sample. Observed Fe II blends at $\lambda 2100$, $\lambda 2500$, $\lambda 2950$, $\lambda 3200$, $\lambda 4570$, $\lambda 5190$, $\lambda 5320$ are also included with mean ratios relative to $\lambda 2500$ blend and a mean ratio of $\lambda 2500$ to Mg II $\lambda 2798$ with the dispersion reported in Table 2 of Grandi (1981).

c) *Lyman Absorption*

A Lyman absorption spectrum is included to study the relation between colors and the physical properties of the intergalactic medium as a function of redshift.

High-resolution spectroscopy shortward of the Lyα emission shows a *forest* of absorption lines interpreted as Lyα produced by intervening hydrogen clouds at redshifts $z_{abs} < z_{em}$ of the Lyα emission (Sargent *et al.* 1980).

According to Oke and Korycansky (1982), we divide into three distinct regions the depression shortward of the Lyα emission:

i) Region A between Lyα and Lyβ 1025 Å emission, where only Lyα lines at $z_{abs} < z_{em}$ are expected under the assumption that all the absorption is due to neutral hydrogen.

ii) Region B between Lyβ and Lyman limit 911 Å where all the Lyman absorption series is present.

iii) Region C shortward of the QSO Lyman limit and containing the Lyman series plus the Lyman continuum absorption.

We express the total absorption in the A and B regions by the parameters D_A and D_B introduced by Oke and Korycansky (1982), representing the mean fraction of flux subtracted from the QSO spectrum in the relevant regions:

$$D_i \equiv \langle 1 - f_{obs}/f_{int} \rangle_i \,, \quad i = \mathrm{A, B} \,, \tag{1}$$

where f_{obs} and f_{int} are the observed and intrinsic fluxes in the observer frame. The average is taken over the wavelength range of the region. Thus for the purpose of computing broadband colors, we model the spectrum depressing by a constant factor D_i the intrinsic QSO flux in each region.

Since the number of hydrogen clouds has been found to increase with redshift, we evaluate the corresponding increase of D_A.

Defining $N(W, z)$ as the number of clouds producing an absorption Lyα of intrinsic (i.e., in the absorber frame) equivalent width W at redshift z, per unit W and z, the resulting depression in region A is

$$D_A \equiv \left(\frac{W_{tot}}{\Delta\lambda}\right)_{obs} = \frac{1}{\Delta\lambda}\int_{z_\beta}^{z_{em}} dz \int_0^\infty dW N(W, z) W(1 + z) \,, \tag{2}$$

where W_{tot} is the observed equivalent width in region A, $\Delta\lambda = (\lambda_{Ly\alpha} - \lambda_{Ly\beta})(1 + z_{em})$ is the observed wavelength range in the same region, and z_β is the redshift where Lyα absorption occurs at the wavelength of QSO emission Lyβ: $1 + z_\beta = (1 + z_{em})\lambda_{Ly\beta}/\lambda_{Ly\alpha}$. It can be shown that $N(W, z)$ can be expressed in the form (Sargent *et al.* 1980; Steidel and Sargent 1987:

$$N(W, z) = \frac{1}{W^*} e^{-W/W^*} N_z(z) \,, \tag{3}$$

where W^* is the mean equivalent width and $N_z = A(1 + z)^\gamma [(1 + z)/(1 + z_{em})]^{-\delta}$ is the number of clouds per unit z. The increase of the cloud number with z is determined by γ, and the last term accounts for the "inverse effect" related to the increasing ionization in the vicinity of the QSO (Hunstead *et al.* 1988). A rough comparison with observations can also be done using the number of clouds at the mean absorption redshift (Steidel and Sargent 1987); in this case, $W_{tot} \simeq N_z(\overline{z_{abs}})\Delta z(1 + \overline{z_{abs}})W^*$, where N_z is the number of clouds at the mean redshift, Δz is the redshift range of the absorbers, and $\Delta\lambda_{obs} \simeq \lambda_{Ly\alpha}\Delta z$ is the corresponding wavelength interval. Therefore,

$$D_A \simeq N_z(\overline{z_{abs}})W^*(1 + \overline{z_{abs}})/\lambda_{Ly\alpha} \,. \tag{4}$$

For our spectrum, we use the Hunstead *et al.* (1988) values: $\gamma = 2.3 \pm 0.38$, $\delta = 2.1 \pm 1.1$. For each z_{em}, we compute the

TABLE 1

CORRELATION PARAMETERS FOR $\log W = b \log L_{30} + a$ ($L_{30} = L/10^{30}$ ergs s^{-1} Hz^{-1})

Lines	b	a	σ
Lyα	−0.15	2.12	±0.16
C IV	−0.27	1.86	±0.24
C III]	−0.12	1.45	±0.20
Mg II	−0.15	1.6	±0.12

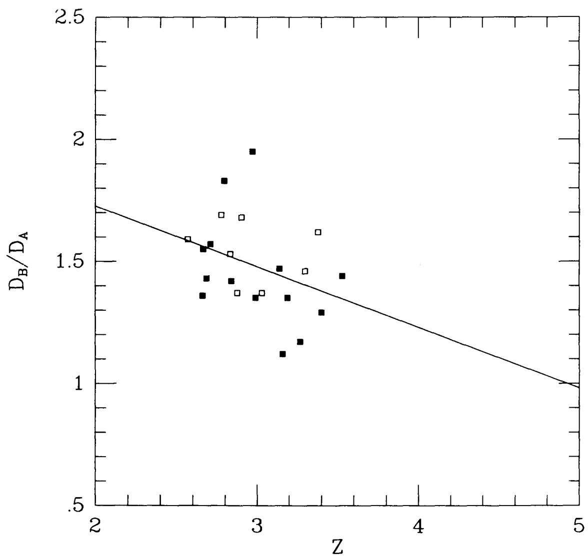

FIG. 1.—The ratio D_B/D_A as a function of redshift: filled squares from Oke and Korycansky (1982); open squares from Steidel and Sargent (1987). The least mean square straight line is also represented.

corresponding average absorption redshift z_{abs} using the evolutionary law to scale the value $N_z = 154 \pm 11$ obtained by Sargent *et al.* (1980) at $\overline{z_{abs}} = 2.44$.

In principle, equation (2) could be applied to compute the mean depression D_B. However, blending due to the presence of the whole Lyman series requires a more accurate analysis, which will be presented elsewhere. For the present analysis, we rely on the observational D_B/D_A values taken from the samples of Oke and Korycansky (1982) and Steidel and Sargent (1987), plotted in Figure 1 as a function of the emission redshift. The two data sets have similar distributions, allowing an unbiased linear regression analysis which gives a correlation coefficient $\rho = 0.35$, significant at $\sim 90\%$ level. The resulting linear fit $D_B/D_A = -0.25z + 2.23$ is used to extrapolate D_B at higher redshifts.

In region C, shortward of the rest frame Lyman limit, we evaluate the average absorption as a function of frequency associating a Lyman absorption edge to each Lyα line. The optical depth at the Lyman limit of each absorbing cloud is the product of the bound-free transition cross section $\sigma_{LL} = 6.3 \times 10^{-18}$ cm^2 times the hydrogen column density $N_{H\,I}$ of the cloud: $\tau_{LL} = \sigma_{LL} N_{H\,I}$. To relate $N_{H\,I}$ with the intrinsic equivalent width W of the corresponding Lyα line, we computed the curves of growth in Figure 2 using a Voigt profile with natural damping only and various values of the Doppler parameter b (Spitzer 1978) obtaining a numerical relation $\tau_{LL} = \tau_{LL}(W)$. For every slice dz, the average intensity decrement $\langle dI_\nu \rangle$ is given by the total intensity times the average attenuation of clouds weighted by the equivalent width distribution:

$$\langle dI_\nu \rangle = I_\nu dz \int dW N(W, z)[1 - e^{-\tau_\nu(W, z)}] , \qquad (5)$$

where $\tau_\nu(W, z)$ is the optical depth at the observed frequency ν produced by the bound-free transitions at redshift z. Since in the cloud rest frame, the optical depth of the Lyman continuum is $\tau_{LL}(\nu_{LL}/\nu_{rest})^3$, the corresponding observed optical depth in equation (5) is

$$\tau_\nu(W, z) = \tau_{LL}(W)\left[\frac{\nu_{LL}}{(1 + z)\nu}\right]^3 , \qquad (6)$$

for all the observed $\nu \geq \nu_{LL}/(1 + z)$.

Thus, integrating in dz along the line of sight, we obtain:

$$\langle I_\nu \rangle = I_0 \exp\left[\!\left[- \int_{z_{min}}^{z_{em}} dz \int dW N(W, z) \times \{1 - e^{-\tau_{LL}(W)[\nu_{LL}/(1+z)\nu]^3}\} \right]\!\right] , \qquad (7)$$

where z_{min} is the redshift where the Lyman limit occurs at the observed frequency ν: $1 + z_{min} = \nu_{LL}/\nu$.

For comparison, we can suppose the same amount of hydrogen contained in the clouds at each redshift as diffused uniformly in a slice dz; this results in a mean number density:

$$n_{H\,I}(z) = \frac{dz}{dl} \int N(W, z) N_{H\,I}(W) dW , \qquad (8)$$

where dl is the proper length interval and $N_{H\,I}(W)$ is the column density determined by the curve of growth. The corresponding optical depth is:

$$\langle \tau_\nu \rangle = \int n_{H\,I} \sigma_{LL}\left[\frac{\nu_{LL}}{(1 + z)\nu}\right]^3 \frac{dl}{dz} dz , \qquad (9)$$

and using equation (8),

$$\langle \tau_\nu \rangle = \int_{z_{min}}^{z_{em}} dz \int dW N(W, z) \tau_{LL}(W)\left[\frac{\nu_{LL}}{(1 + z)\nu}\right]^3 . \qquad (10)$$

This allows the Gunn and Peterson (1965) test for the Lyman continuum. The emerging intensity proportional to $e^{-\langle \tau_\nu \rangle}$ is lower with respect to the case of discrete clouds proportional to $\langle e^{-\tau_\nu} \rangle$ and represents an upper limit to the absorption of hydrogen for a given curve of growth.

To evaluate the average absorption due to the Lyα spectrum of the cloud system, we have to consider the different properties of lines having small or large intrinsic equivalent width. Indeed, the absorption in region A, where only Lyα lines are present, is dominated by the large number of small equivalent width lines ($W_{Ly\alpha} \lesssim 0.5$ Å), whose column density is almost independent of any reasonable value of the Doppler parameter b. On the contrary, in region C most of the absorption comes from the small fraction of high column density clouds (with $W_{Ly\alpha} \lesssim 2$ Å and $N_{H\,I} \sim 10^{18}$ cm^{-2}), which are usually associ-

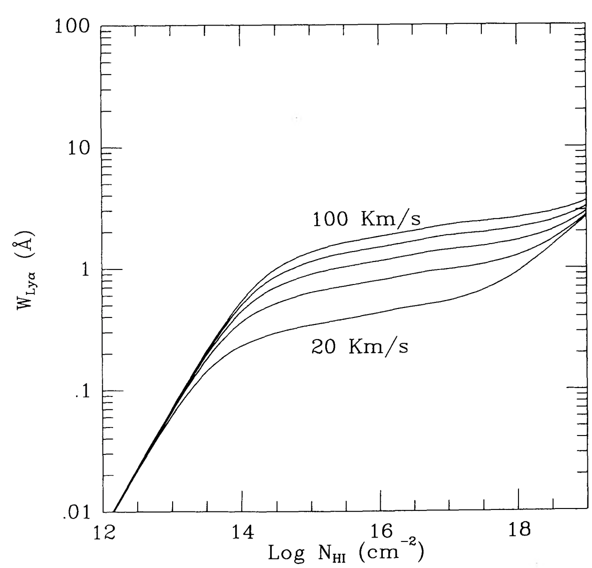

FIG. 2.—Curves of growth for the Lyα line computed for different values of the Doppler parameter b = 20, 40, 60, 80 100 km s^{-1}.

ated with metal line systems (Sargent *et al.* 1980). Since these lines are saturated, a small error in W causes a larger uncertainty in column density. Indeed, individual lines may be affected by blending, preventing a determination of $N_{\rm H\,I}$ (see Bechtold 1987). In principle, the correspondence $W - N_{\rm H\,I}$ may be established in a statistical sense if the *deblended* equivalent width distribution (see Sargent *et al.* 1980) is known. However, blending effects are not definitely quantified, so the relation between the mean Lyman continuum absorption and the average Doppler parameter of the absorbers relies on the *assumed* $N(W, z)$.

Metal line systems are known to have a slower cosmological evolution. So we divide the equivalent width spectrum into a population of Lyα lines with $N_{\rm H\,I} \lesssim 10^{16}$ cm^{-2}, with the evolution typical of the Lyα forest (Hunstead *et al.* 1988) and a population of "metal Lyα" with an evolution proportional to $(1 + z)^{0.68}$ derived from Sargent, Steidel, and Boksenberg (1989) and an upper limit for the equivalent width of 2 Å. Stronger Lyman limit absorptions by damped systems exist but are rare and better treated as individual edges possibly added to the average absorption.

d) The Resulting Spectrum

In Figure 3, we show an example of a spectrum obtained combining an emission-line spectrum, a hydrogen absorption spectrum, and continuum emission as described in previous paragraphs. Line intensities are obtained according to the Baldwin correlation for a continuous luminosity $L \sim 2 \times 10^{30}$ ergs s^{-1} Hz^{-1} at 2500 Å. Lyman continuum absorption is obtained using equation (7) and associating a curve of growth with $\langle b \rangle = 60$ km s^{-1} to the stronger Lyα lines. The overall spectrum is then shown in the rest frame frequency for various redshifts.

Beyond the QSO Lyman limit, the steepness of the absorption increases for two combined effects: the increase of the number of clouds per unit redshift and the increase of the redshift interval corresponding to a given dv:

$$\frac{d\tau}{dv} = \frac{d\tau}{dz}\frac{dz}{dv} = \frac{d\tau}{dz}\frac{1+z}{v} , \tag{11}$$

where v is the observed or the rest frame frequency indifferently.

However, shortward of $\lambda_r \sim 500$ Å, the spectrum recovers with a steepness depending on the adopted continuum emission and increasing for higher QSO redshifts.

For comparison in Figure 3, the absorption due to a continuum distribution of the same amount of hydrogen, for a $z = 3$ QSO, is also shown. This represents the upper limit to the absorption produced by a given hydrogen density $n_{\rm H\,I}$.

We note that applying the steeper redshift evolution of the Lyα forest to the metal line systems would produce an appreciably stronger absorption for $z > 3$ ($\sim$ a factor 10 at $\lambda \sim$ 600 Å for $z_{\rm em} = 5$) for a given Doppler parameter b.

For a given $N(W, z)$, even small variations on the adopted b of the clouds produces large variations in the observed flux, especially for high-redshift QSOs (see Fig. 4).

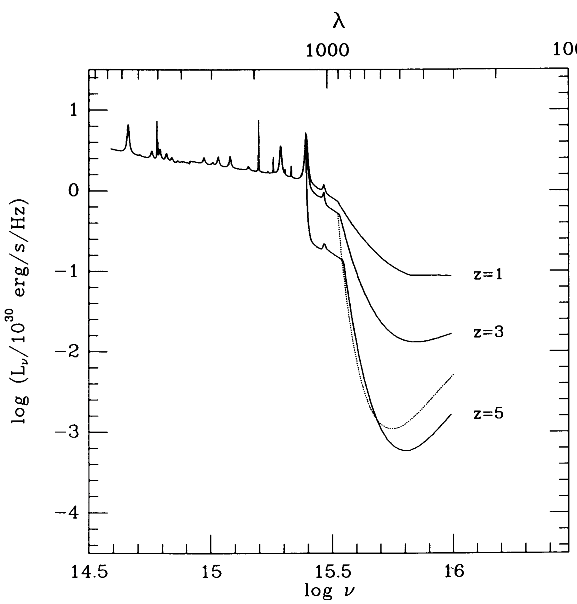

FIG. 3.—A model QSO spectrum, as described in the text, computed for an average cloud temperature corresponding to $b = 60$ km s^{-1} and redshifts $z = 1, 3, 5$ (*solid lines*). The dotted line represents the spectrum of a $z = 3$ QSO, assuming the hydrogen of the clouds uniformly distributed at each redshift.

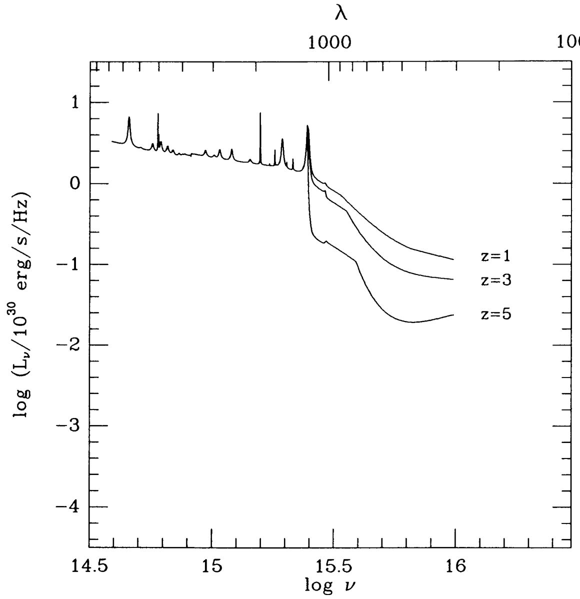

FIG. 4.—A model QSO spectrum as in Fig. 3, but with Lyα absorption computed for a higher temperature corresponding to $b = 70$ km s^{-1}.

III. THE REDSHIFT DEPENDENCE OF BROAD-BAND COLORS

The model spectrum described in the previous section has been redshifted at various z values and then integrated in the standard Johnson bands, in the photographic bands used by Kron (1980) (see also Koo 1986) and by Warren *et al.* (1987*a*). Zero point magnitudes are determined from the Vega spectrum as obtained by Hayes and Latham (1975), assuming zero color indices. A standard Friedmann cosmology is assumed with $q_0 = 0.1$ to compute apparent magnitudes and to correlate emission-line equivalent widths with absolute magnitude according to the Baldwin correlation.

Since our aim is the analysis of biases in the color selection of QSOs, we examine first the QSO paths in the color-color diagrams $(U-J, J-F)$ and $(J-F, F-N)$ used by Koo and Kron (1988) and Marano, Zamorani, and Zitelli (1988) to select faint complete samples of candidates.

Colors are not strongly affected by changes in the continuum emission. For example, even a change $\Delta\alpha = 0.5$ in the power-law index leads to a change in colors $\lesssim 0.2$ mag only. The other major component, the big bump, extending from 5500 to $\lesssim 1000$ Å, appears simultaneously in UJF bands up to $z = 2$. Thus, adding to the power-law spectrum a blue bump which enhances the emission at 2500 Å by a factor of 2 changes the colors by ~ 0.1 mag for $1 < z < 2$; at lower z, the change is $\lesssim 0.2$ mag.

Up to $z \lesssim 3$, variations of emission-line intensities affect the QSO paths as shown in Figure 5. Baldwin correlation implies that brighter QSOs have weaker line intensities, causing smaller color changes with redshift.

Note that up to $z \sim 2.3$, the line intensities do not affect the Koo and Kron (1982) color selection, since the QSO paths are well outside the stellar locus in the UJF diagram, while the ultraviolet excess selection could be biased against strong lined objects.

A quantitative estimate of these biases will be discussed on statistical grounds in the next section.

Beyond $z \sim 2.5$, intervening hydrogen absorption enters progressively the UJF bands determining the apparent colors. In regions A and B, some statistical data on Lyα absorption lines do exist, while beyond the Lyman limit spectroscopic data do not allow any reliable statistics on the QSO colors. In this region, the intensity is often depressed to undetectable levels at frequencies beyond the first Lyman edge; this is consistent with the predictions of our model. Hence, we cannot estimate the expected completeness levels of very high redshift color surveys (e.g., Warren, Hewett, and Osmer 1988). However, our simplified model gives some useful qualitative indications on the relation between the statistics of Lyα clouds and the average paths in color-color diagrams.

Figure 6 shows different paths in color-color diagrams resulting from an average emission spectrum and different values of the Doppler parameter of the clouds.

For example, for $b = 50$ km s^{-1}, the resulting strong absorption brings average QSOs with $z \gtrsim 3.5$ well outside the stellar locus.

For $b \gtrsim 60$ km s^{-1}, the QSO path lies inside or very near the stellar locus for $3 \lesssim z \lesssim 4$, especially in the UJF diagram. In this case, quasars would be lost by color selection techniques.

For $b \gtrsim 70$ km s^{-1}, the $U-J$ color is always $\lesssim 0$, and for $z \gtrsim 3.3$, QSOs come out of the stellar locus on the red $J-F$ side.

Note that a decrease of b can be balanced by a correction for line blending, which tends to reduce the apparent number of high-W clouds. Thus, the b values shown in Figure 6 are not a true measure of the average Doppler parameter of the absorbers but simply serve as indicators of trends in color space.

In Figures 7a and 7b, very high redshift QSOs are shown in color-color diagrams. Three out of four appear consistent with low b values. On the other hand, absorption in the UV part of the spectrum depends on the random occurrence of a few strong absorbers along the line of sight, which produces a large dispersion in colors. Thus, we cannot say whether these objects are consistent with an average strong absorption or represent the tail of a distribution corresponding to a weaker average absorption. We can only say that a higher average Doppler parameter of the absorbers produces a larger incompleteness of color-selected QSO samples.

In Figure 8, we show K-corrections for the same models as in Figure 6:

$$\Delta m_i = 2.5 \log (1 + z) - 2.5 \log \frac{\int L[\nu(1 + z)]\phi_i(\nu)d\nu}{\int L(\nu)d\nu}, \quad (12)$$

where ϕ_i is the overall transmission for each of the $UJFN$

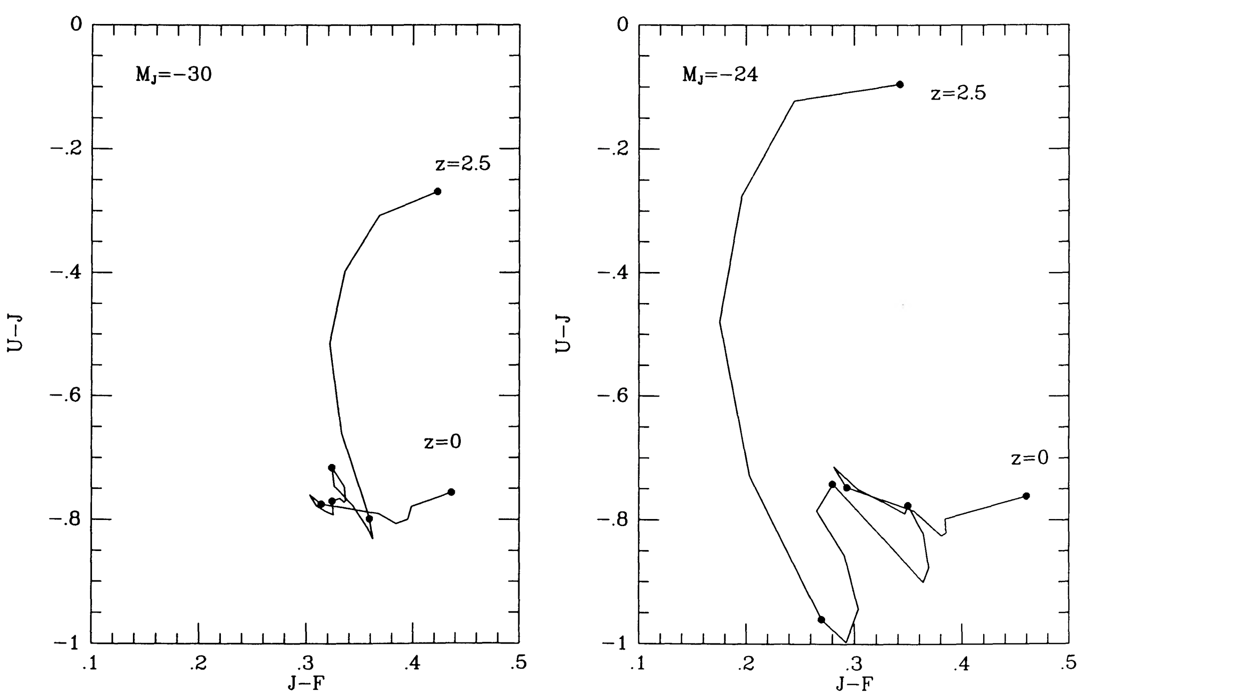

FIG. 5.—QSO paths in $U-J$ vs. $J-F$ diagrams computed for objects of magnitude $M_J \sim -30$ and $M_J \sim -24$. Dots indicate redshifts in steps of 0.5 starting from $z = 0$. Comparison of two paths shows the effect of the Baldwin correlation.

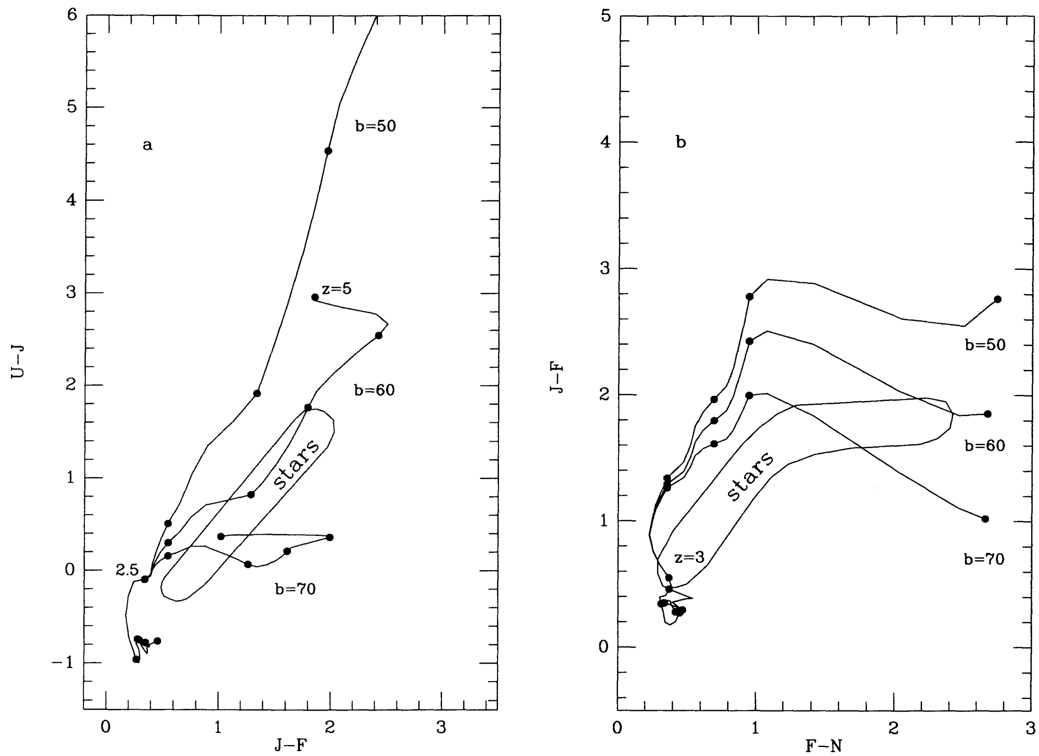

FIG. 6.—Paths in color-color diagrams for different values of the Doppler parameter, computed for a QSO of $M_J \sim -24$. Dots have the same meaning as in Fig. 5. A schematic representation of the stellar locus is also plotted.

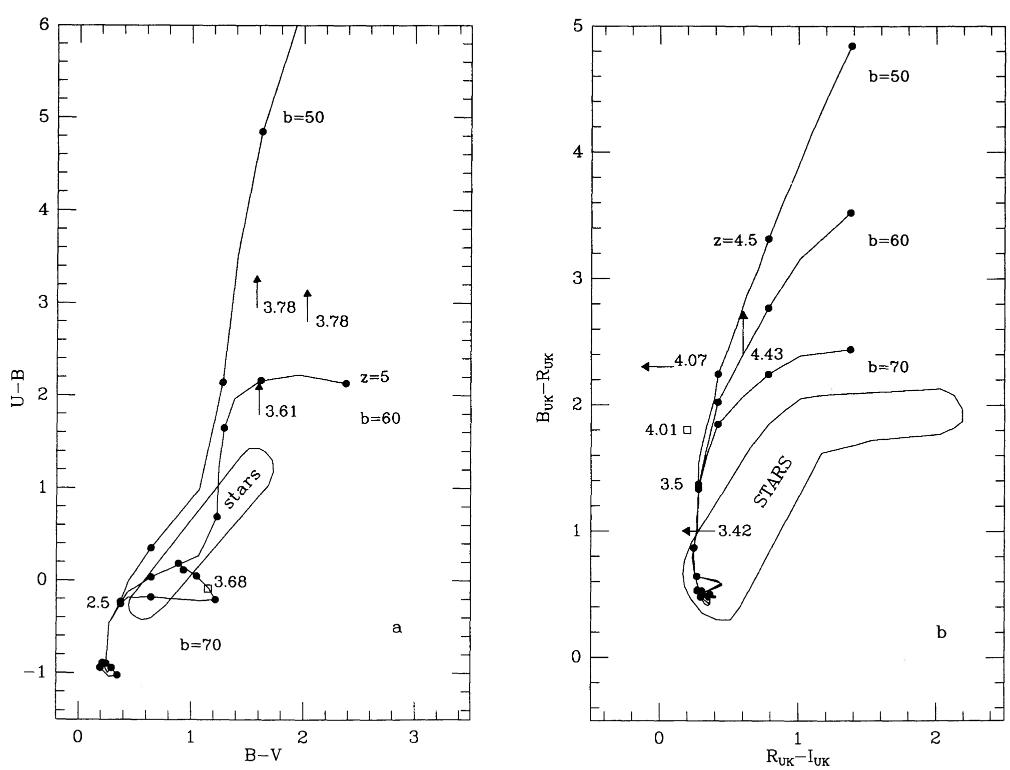

FIG. 7.—QSO paths in two-color diagrams for different values of the Doppler parameter. The standard Johnson and UK Schmidt colors are used. Dots indicate redshifts as in Fig. 6. The schematic stellar loci are also shown. The high-z QSOs reported by Savage *et al.* (1987) are shown in (*a*); those reported by Warren *et al.* (1987*a*, *b*) are shown in (*b*). Arrows indicate lower limits.

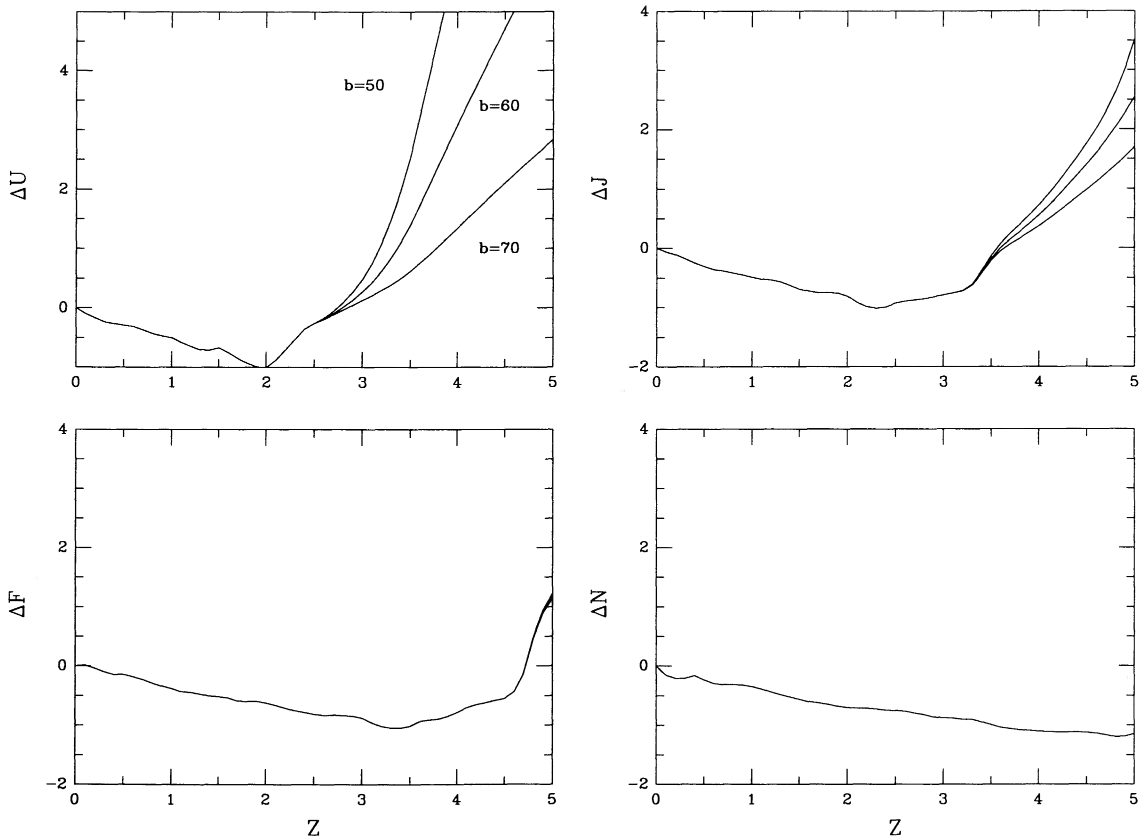

FIG. 8.—K-corrections as a function of redshift for $UJFN$ bands computed for different average cloud temperatures as in Fig. 6

bands. We note that this correction blows up for $z \gtrsim 3$ in the U band and at correspondingly higher redshifts in JFN bands. Consequently, high-z objects become extremely faint and can be lost by blue flux limited surveys, even if their colors are definitely nonstellar. In any case, statistics of high-redshift objects, which are more easily detected in red bands, should also be referred to red magnitudes for which K-corrections are smaller and less uncertain.

The highest redshift QSOs which have been found by Warren *et al.* (1987*a*) with a multicolor technique, have a surface density $\lesssim 1$ deg^{-2} for $R < 20$ and $3 < z < 4$ (Warren *et al.* 1988). For comparison, we consider models of pure luminosity evolution of the type $L \propto \exp(kT)$ (where T is the look-back time), fitted to the Boyle, Shanks, and Peterson (1988) luminosity function (LF) as in Cavaliere *et al.* (1988). Apart from K-correction, when more and more distant QSOs are observed, the sliding down along the bright and steep end of the LF appears in the z distribution at $B \lesssim 21$ and $z \gtrsim 2$, causing an intrinsic decrease in the number of expected high-redshift QSOs. For example, we expect ~ 5 deg^{-2} for $3 < z < 4$. The expected decrease is still insufficient to explain the observed number, and this would require the introduction of a birth function for the QSO population at $z \gtrsim 3$. However, a lower average absorption, shifting QSOs toward the stellar locus, would increase the incompleteness of multicolor samples reducing the discrepancy. The incompleteness could also affect red counts as far as the selection involves bluer colors.

Complementary methods as radio selection, emission-line and variability, which is also efficient as a selection technique (Trevese *et al.* 1989), becomes essential in this redshift range. Broad-band colors of large numbers of objects selected by these methods could give statistical information on properties of the absorbers and their cosmological evolution.

It should be noted that the transit grism surveys of Schmidt, Schneider, and Gunn (1987) found ~ 0.5 deg^{-2} brighter than $r = 20$ which is roughly consistent with the color selection of Warren, Hewett, and Osmer (1988). However, the spectroscopically selected objects show an average emission Lyα of unusually high equivalent width ($W_r \sim 90$ Å). It is difficult to understand if this is due simply to a bias of the survey against weak emission-line objects or if it is an indication of spectral evolution in the QSO population. In any case, comparisons of the completeness levels of broad-band flux-limited and line flux-limited surveys remains a problematic task.

IV. COLOR STATISTICS

For $z \lesssim 3$, broad-band colors $UJFN$ are affected mainly by the emission-line spectrum as discussed in the previous section; in particular, the ultraviolet band is not affected by Lyman continuum absorption. On the other hand, statistics on the equivalent widths of the main emission lines are now available from complete samples (see § II).

Thus, we computed a "modal" spectrum corresponding to the set of most probable values of the parameters involved. We also changed the parameters according to their statistical distributions and possible correlations using a Monte Carlo simulation. Then, magnitudes in various photometric bands have been determined for each spectrum adding random photometric errors. Finally, a statistical distribution of colors has been derived.

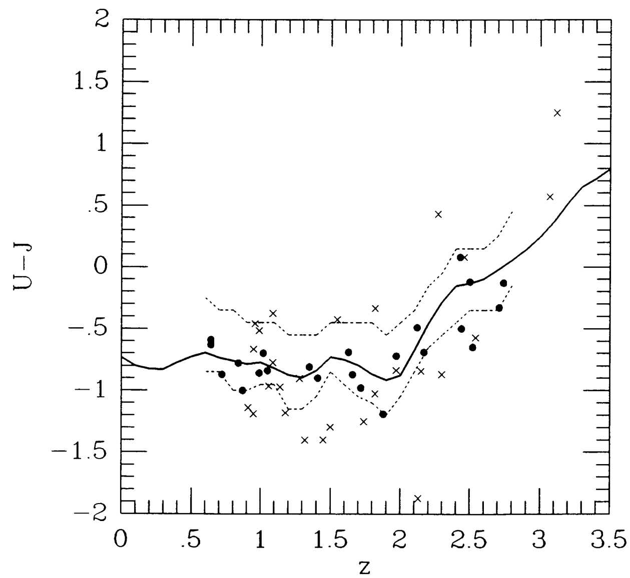

FIG. 9.—$U-J$ color as a function of redshift. The solid line corresponds to the "modal" QSO spectrum. The dotted lines represent 90% confidence contour as derived from Monte Carlo simulations. Crosses and solid dots are QSOs from the KKC and MZZ samples, respectively.

Special classes of objects such as BAL QSOs with broad absorption features are not included in the present analysis. Damped Lyα systems are also excluded.

Since line statistics include the Baldwin correlation, average colors depend on the luminosity. Therefore, color distributions are computed for objects in a fixed interval of apparent magnitudes to represent actual color surveys where comparison between high- and low-z objects involves different luminosities.

Figures 9–10 show colors of the modal spectrum as a function of z. Dotted lines represent a 90% confidence level as obtained from the Monte Carlo color distributions. We restrict the comparison to complete multicolor samples to avoid biases in the statistical color distributions of general QSO catalogs, affected by various selection effects. The model is compared with the deep complete surveys of Koo, Kron, and Cudworth (1986, KKC) and Marano, Zamorani, and Zitelli (1988, MZZ), which have photometric errors ($\sigma_m \sim 0.05$) smaller than the intrinsic color spread.

We note that confidence intervals are not symmetric with respect to the modal QSO, in agreement with the observed color distribution.

The larger scatter in $U-J$ of the KKC sample is due in part to the intrinsic variability of QSOs. In fact, the J and F plates used by KKC were taken at the same epoch, while U plates were taken 5 years later.

Two out of 23 MZZ objects lie outside the 90% contours in Figure 9, and five out of 50 MZZ plus KKC objects lie outside the contours in Figure 10. This means that our simulation produces both the correct modal colors and their dispersions. We stress that the statistical data used for the synthetic spectrum are based on a sample which is independent of those of KKC and MZZ; thus, the agreement found shows that these samples have the same average spectral properties.

Note that $J-F$ is fairly constant, within the overall spread, up to $z \sim 3$, while $U-J$ is more sensitive to the redshifted ultraviolet emission lines and for $z \gtrsim 2.5$ shows a steep increase due to the Lyman continuum absorption in agreement with colors of the highest redshift QSOs presently known (see also Warren, Hewett, and Osmer 1988).

The statistical distribution of colors can be used to estimate the completeness levels at each z value for surveys based on color selection.

Let us consider first the Boyle, Shanks, and Peterson (1988) ultraviolet excess survey ($U-B \lesssim -0.3$). The reddening produced by Mg II and C IV passing through the B band causes the loss of a small ($\lesssim 10\%$) fraction of QSOs at redshift $z \sim 0.5$ and $z \sim 1.5$, respectively (Fig. 11). At $z \gtrsim 2.2$, the UVX surveys become substantially incomplete because of the reddening produced by Lyα drift from U to B bands. However, in rich enough samples, such as Boyle, Shanks, and Peterson, a few objects are expected up to $z \sim 3$ due to $U-B$ scattering, both intrinsic and photometric. At $z \gtrsim 2.2$, our color distribution,

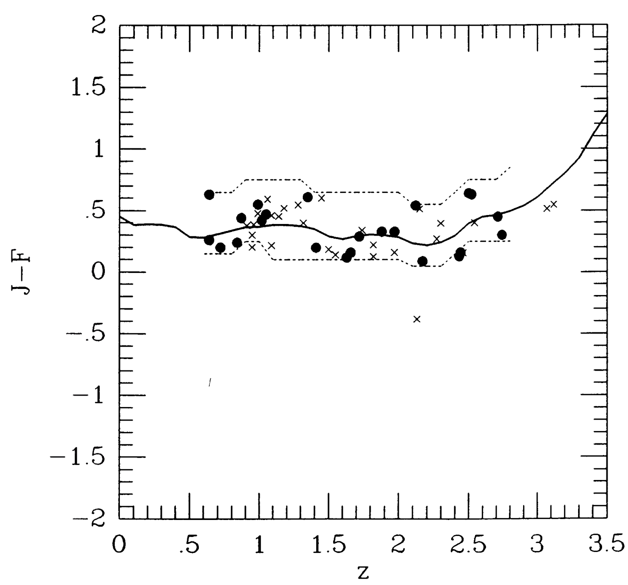

FIG. 10.—$J-F$ color as a function of redshifts. The meaning of the symbols is the same as in Fig. 9.

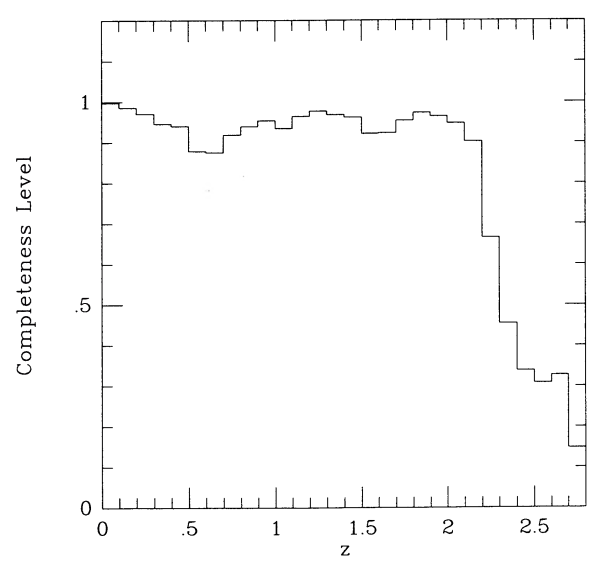

FIG. 11.—Completeness level as a function of redshift for the Boyle, Shanks, and Peterson (1988) sample, as deduced by the Monte Carlo simulation. The drop at $z \gtrsim 2.2$ is due to the drift of Lyα line from U to B band.

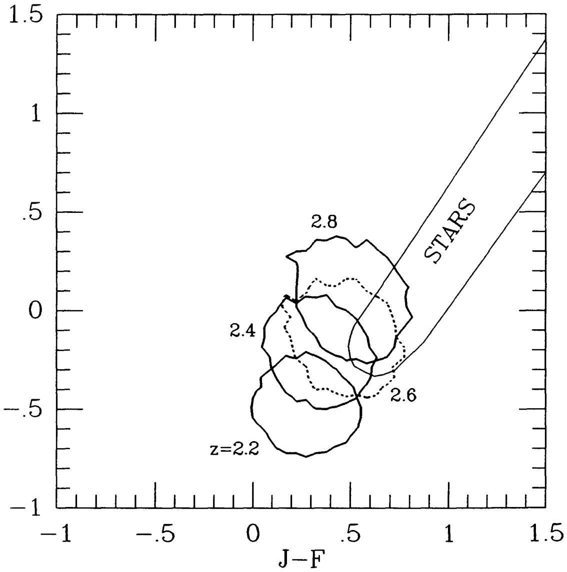

FIG. 12.—Contours of 90% probability in color-color diagram as obtained by Monte Carlo simulations for different values of redshift. The stellar locus is also indicated.

including photometric errors as stated in Boyle, Shanks, and Peterson (1988), gives a slope $d\phi/dz \simeq 2.5$. The expected decline of the fraction ϕ of selected objects at each z is $d\phi/dz = d\phi/d(U-B)d(U-B)/dz$.

At $z \sim 2.4$, where the average QSO color crosses the UVX threshold, we have $d(U-B)/dz \simeq 1$; even in the absence of intrinsic dispersion, assuming a Gaussian distribution in the photometric errors, we have $d\phi/dz \simeq d\phi/d(U-B) = 1/(\sigma\sqrt{2\pi})$. Assuming an rms color error as small as $\sigma = 0.1$ mag, we have $d\phi/dz \simeq 4$. On the other hand, from the redshift distribution of Boyle, Shanks, and Peterson sample the corresponding slope is larger by a factor of 2, suggesting the presence of a further selection besides UVX. This should be a spectroscopic bias acting at $z \simeq 2.2$.

To reduce the incompleteness at $z \gtrsim 2$, Koo and Kron (1982) introduced a different color selection which assumes to be QSO candidates all objects which lie well outside the stellar locus in the $U-J$ versus $J-F$ plane.

We have used our synthetic color distribution to estimate the completeness level also in this case. In Figure 12, 90% probability contours are shown for various redshifts. We confirm that this color selection is definitely successful in picking up all QSOs with $z \lesssim 2.2$. However, at higher z, some incompleteness appears, reaching a maximum at about $z \sim 2.6$ being 5%, 30%, 26% at $z = 2.4$, 2.6, 2.8, respectively, depending of course on the details of the stellar color boundary adopted. Lost objects are those with weaker emission lines appearing in the J band as Lyα.

Global counts are not appreciably altered by these rather "localized" losses, which can, however, affect our understanding of the cosmological evolution of the luminosity function for $z \gtrsim 2.5$.

Since for $z \gtrsim 3$ Lyman limit absorption enters the U band, the $U-J$ color is mainly determined by the poorly known properties of the absorbing medium, preventing any statistical correction.

V. SUMMARY

We have developed a model QSO spectrum which includes the main features of the continuum and the main emission lines. We have used the available statistics of these spectral parameters to generate a distribution of broad-band colors via a Monte Carlo simulation.

Since the ultraviolet region of the spectrum is strongly affected by absorption of intervening hydrogen clouds, we have also modeled the absorption due to hydrogen lines using Lyα forest statistics. This allows the prediction of colors, including the U band, up to $z \lesssim 2.8$.

We have also modeled the Lyman limit absorption to explore the effect of the average Doppler parameter of the absorbers on the average QSO colors.

The main results of the present analysis are the following.

1. For $z \lesssim 2.8$, our color distribution is in good agreement with the MZZ and KKC faint surveys. Since the statistics comes from a completely independent sample, this agreement shows a consistency in the spectral properties.

2. Our synthetic color distribution allows us to estimate the incompleteness of the various color selection methods as a function of redshift. As is well known, two-color selection technique is efficient in finding QSOs also at $z \gtrsim 2$, where the UVX criterion fails. However, local incompleteness at $z \sim 2.6$ can be as high as 30% due to QSOs lost in the stellar locus.

3. The scarcity of information on the physics of the absorbing clouds prevents any statistical prediction on colors affected by Lyman continuum absorption for $z \gtrsim 2.8$. In fact, the high-redshift objects found so far could be either consistent with an average strong absorption or could be the tail of a weaker absorption distribution. In any case, weaker average absorption would imply a larger incompleteness of color-selected samples, due to the larger fraction of high-z QSOs with stellar colors.

4. An estimate of the intrinsic QSO redshift distribution suffers some incompleteness at medium redshifts in UVX and color-color surveys, and it could be considerably altered at $z \gtrsim 3$ by the loss of weakly absorbed QSOs, making premature any interpretation of the observed decline at high z values in terms of QSO birth.

It is a pleasure to acknowledge informative discussions with A. Cavaliere, R. G. Gratton, B. Marano, and V. Zitelli. We are indebted to the referee for critical comments on the analysis of the Lyman absorption. Work performed under grants from MPI and CNR (GNA).

REFERENCES

Baldwin, J. A., Wampler, E. J., and Gaskell, C. M. 1989, *Ap. J.*, **338**, 630.

Bechtold, J. 1987, in *High Redshift and Primeval Galaxies*, ed. J. Bergeron, D. Kunth, B. Rocca-Volmerange, and J. Tran Thanh Van (Gif sur Yvette: Editions Frontières), p. 397.

Boyle, B. J., Shanks, T., and Peterson, B. A. 1988, *M.N.R.A.S.*, **235**, 935.

Braccesi, A., Formiggini, L., and Gandolfi, E. 1970, *Astr. Ap.*, **5**, 264.

Cavaliere, A., Giallongo, E., Padovani, P., and Vagnetti, F. 1988, in *Proc. Workshop on Optical Surveys for Quasars*, ed. P. S. Osmer, A. C. Porter, R. F. Green, and C. B. Foltz (ASP Conf. Series, Vol. **2**), p. 335.

Elvis, M. 1986, in *IAU Symposium 119, Quasars*, ed. G. Swarup and V. K. Kapahi (Dordrecht: Reidel), p. 73.

Grandi, S. A. 1981, *Ap. J.*, **251**, 451.

Grandi, S. A. 1982, *Ap. J.*, **255**, 25.
Gunn, J. E., and Peterson, B. A. 1965, *Ap. J.*, **142**, 1633.
Hayes, D. S., and Latham, D. W. 1975, *Ap. J.*, **197**, 593.
Hazard, C., and McMahon, R. G. 1985, *Nature*, **314**, 238.
Hunstead, R. W., Murdoch, H. S., Pettini, M., and Blades, J. C. 1988, *Ap. J.*, **329**, 527.
Koo, D. C. 1986, *Ap. J.*, **311**, 651.
Koo, D. C., and Kron, R. G. 1982, *Astr. Ap.*, **105**, 107.
———. 1988, *Ap. J.*, **325**, 92.
Koo, D. C., Kron, R. G., and Cudworth, K. M. 1986, *Pub. A.S.P.*, **98**, 285 (KKC).
Kron, R. G. 1980, *Ap. J. Suppl.*, **43**, 305.
Malkan, M. A. 1983, *Ap. J.*, **268**, 582.
Malkan, M. A., and Sargent, W. L. W. 1982, *Ap. J.*, **254**, 22.
Marano, B., Zamorani, G., and Zitelli, V. 1988, *M.N.R.A.S.*, **232**, 111 (MZZ).
Miller, L., and Mitchell, P. S. 1988, in *Proc. Workshop on Optical Surveys for Quasars*, ed. P. S. Osmer, A. C. Porter, R. F. Green, and C. B. Foltz (ASP Conf. Series, Vol. **2**), p. 114.
Oke, J. B., and Korycansky, D. G. 1982, *Ap. J.*, **255**, 11.
Osmer, P. S., and Smith, M. G. 1980, *Ap. J. Suppl.*, **42**, 333.
Richstone, D. O., and Schmidt, M. 1980, *Ap. J.*, **235**, 361.
Sargent, W. L. W., Steidel, C. C., and Boksenberg, A. 1989, *Ap. J. Suppl.*, **69**, 703.
Sargent, W. L. W., Young, P. J., Boksenberg, A., and Tytler, D. 1980, *Ap. J. Suppl.*, **42**, 41.
Savage, A., *et al.* 1987, in *IAU Symposium 124, Observational Cosmology*, ed. A. Hewitt, G. Burbidge, and Fang Li Zhi (Dordrecht: Reidel), p. 673.
Schmidt, M. 1968, *Ap. J.*, **151**, 393.
Schmidt, M., Schneider, D. P., and Gunn, J. E. 1987, *Ap. J.* (*Letters*), **316**, L1.
Spitzer, L., Jr. 1978, *Physical Processes in the Interstellar Medium* (New York: Wiley).
Steidel, C. C., and Sargent, W. L. W. 1987, *Ap. J.*, **313**, 171.
Trevese, D., Pitella, G., Kron, R. G., Koo, D. C., and Bershady, M. 1989, *A.J.*, **98**, 108.
Véron, P. 1983, in *Quasars and Gravitational Lenses*, ed. J. P. Swings (Liège: Institut d'Astrophysique), p. 210.
Warren, S. J., Hewett, P. C., Irwin, M. J., McMahon, R. G., Bridgeland, M. T., Bunclark, P. S., and Kibblewhite, E. J. 1987*b*, *Nature*, **325**, 131.
Warren, S. J., Hewett, P. C., and Osmer, P. S. 1988, in *Proc. Workshop on Optical Surveys for Quasars*, ed. P. S. Osmer, A. C. Porter, R. F. Green, and C. B. Foltz (ASP Conf. Series, Vol. **2**), p. 96.
Warren, S. J., Hewett, P. C., Osmer, P. S., and Irwin, M. J. 1987*a*, *Nature*, **330**, 453.

EMANUELE GIALLONGO: Osservatorio Astronomico di Roma, I-00040 Monteporzio, Italy

DARIO TREVESE: Istituto Astronomico di Roma, via Lancisi 29, I-00161 Roma, Italy